Magnetic Bragg peak enhancement under ultrasound injection

Shin-ichi Shamoto [1,2,3,4,*] Mitsuhiro Akatsu [5] Masato Matsuura [1] Seiko Ohira-Kawamura,[6] Kazuya Harii,[7] Masao Ono,[3]
Lieh-Jeng Chang,[2] Takashi U. Ito,[3] Yuichi Nemoto,[8] and Jun'ichi Ieda [3]

[1]*Neutron Science and Technology Center, Comprehensive Research Organization for Science and Society, Tokai, Ibaraki 319-1106, Japan*
[2]*Department of Physics, National Cheng Kung University, Tainan 70101, Taiwan*
[3]*Advanced Science Research Center, Japan Atomic Energy Agency, Tokai, Ibaraki 319-1195, Japan*
[4]*Meson Science Laboratory, RIKEN, Wako, Saitama 351-0198, Japan*
[5]*Department of Physics, Niigata University, Niigata, Niigata 950-2181, Japan*
[6]*J-PARC Center, Japan Atomic Energy Agency, Tokai, Ibaraki 319-1195, Japan*
[7]*Department of Functional Materials Research, National Institutes for Quantum Science and Technology, Takasaki, Gunma 370-1292, Japan*
[8]*Graduate School of Science and Technology, Niigata University, Niigata, Niigata 950-2181, Japan*

Ultrasound injection effect on a magnetic Bragg peak of yttrium iron garnet has been studied by quasielastic neutron scattering. The magnetic Bragg peak is vastly enhanced with decreasing temperature. The energy width increases proportionally to the square root of the sample temperature increase induced by the ultrasound injection. Based on a liquid model, the estimated effective mass becomes light when magnetic domain walls are removed under a magnetic field. Because the magnetic Bragg peak is enhanced by the lattice vibration, the enhancement is expected to closely relate to the spin-lattice coupling. The sharp drop is observed above 100 K for the longitudinal mode, indicating the degradation of the spin-lattice coupling. It is consistent with the suppression of the spin Seebeck effect when the temperature rises above 100 K, demonstrating the spin-lattice coupling as the degradation mechanism.

I. INTRODUCTION

Bragg reflection of a high-quality Si crystal is largely enhanced by ultrasound (US) injection. With increasing the US amplitude, the peak intensity first increases, as explained by the loss of Pendellösung oscillations due to the lattice gradient [1]. Then, the rocking-curve width becomes wide. The integrated intensity increases first linearly, then saturates with the US amplitude. The behavior can be simulated based on a linear gradient crystal model [1]. The reflection curve of a perfect crystal is expressed by the dynamical theory of diffraction [2]. Neutron spin-echo spectroscopy is used on a Si crystal to distinguish the elastic and inelastic scattering components [3]. The injected US leads to phonon creation in Si for both longitudinal and transverse US modes [3]. The US injection can be regarded as a phonon injection based on this conclusion. A neutron backscattering spectrometer on Ge crystal [4] has also been used to investigate the US injection effect, where the reflectivity becomes comparable to that of the graphite deflector. In terms of a magnetic system, the US injection effect has yet to be investigated using neutron scattering.

US injection can also induce a spin current in a magnetic insulator yttrium iron garnet (YIG) as an acoustic spin pumping in a platinum film attached to the YIG [5–8] that can be detected through an inverse spin Hall effect (ISHE) [9,10]. The spin Seebeck effect (SSE), a generation of a spin current by a temperature gradient, has been extensively studied [11,12]. In contrast to the positive spin Seebeck voltage created by the temperature gradient, the SSE voltage induced by the ultrasonic injection into YIG has a negative sign [5]. Moreover, the magnetic field dependence of the SSE shows an enhancement at a certain magnetic field where the dispersions of magnon and phonon hybridized forming magnon-polaron (or magnetoelastic wave) [12]. The enhanced spin Seebeck voltage shows a peak in the temperature range between 50 and 100 K, then decreases with increasing temperature for both longitudinal and transverse modes [13]. The SSE is greatly reduced at low temperatures due to the decrease in magnon thermal excitation, whereas the decrease near room temperature is related to spectral nonuniformity of the magnon thermalization lengths in the thermospin conversion [12] and magnon-magnon scattering [14]. Below 150 K, the magnetization of YIG is slightly suppressed, implying spin canting [15]. In the temperature range, the quantum magnetoelectric effect is also observed [16]. To address those issues, in this study, we conduct neutron scattering experiments in a wide range of temperatures.

The time-of-flight (TOF) near-backscattering spectrometer DNA (BL02) at Japan Proton Accelerator Research Complex (J-PARC) Materials Life Science Experimental Facility
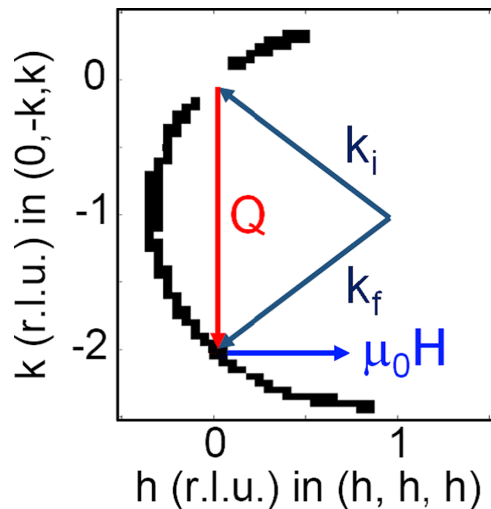
FIG. 1. Horizontal scattering plane in a typical experimental setting at DNA spectrometer. **Q** is the scattering vector of (0, 2, –2). Magnetic field μ_0**H** is applied normal to **Q**. Black jagged semicircles are Q regions covered by detectors.

FIG. 2. Schematic sample cell configuration used for neutron scattering and spin Seebeck effect. YIG crystal rod glued with $LiNbO_3$ transducers on both ends was set on two aluminum pillars with a temperature sensor Cernox. A pair of permanent magnets were placed on the copper frame covered by permalloy tape. The sample cell was surrounded by cadmium plates to reduce the background for neutron scattering.

(MLF) achieves high-energy resolution down to 1.6 μeV, which corresponds to 390 MHz [17]. The frequencies employed in the US measurements [3] are comparable to this resolution. Furthermore, unlike a neutron spin-echo spectrometer, this spectrometer can perform neutron scattering measurements of ferromagnets such as YIG in a magnetic field. Here, we have studied the US injection effect on a magnetic Bragg peak $02\bar{2}$ of YIG, mainly using the backscattering spectrometer DNA. The results of the quasielastic neutron scattering (QENS) will be shown. Then, as a useful tool for measuring the spin-lattice coupling, this combination approach of neutron scattering and US injection will be discussed.

II. EXPERIMENTAL PROCEDURES

YIG crystals were grown with a diameter of about 5.5 mm along [1 1 1] and [0 0 1] directions by a traveling solvent floating zone furnace [18] with four halogen lamps (FZ-T-4000-H-II-S-TS, Crystal Systems Co., Ltd.). The crystal directions were within 3 degrees in the accuracy. In YIG, the [1 1 1] is an easy magnetization axis, whereas the [0 0 1] is a hard magnetization axis. YIG crystallographic symmetry was approximated to be a cubic symmetry [19] of a space group $Ia\bar{3}d$ (#230) with a lattice parameter $a = 12.38$ Å at 300 K. The chemical composition is $Y_{2.84\pm0.09}Fe_5O_{11.57\pm0.21}$, determined by a single-crystal neutron diffraction analysis [20].

Neutron scattering measurements of YIG crystals were carried out by a near-backscattering TOF spectrometer DNA (BL02) [17] and cold-neutron disk-chopper spectrometer AMATERAS (BL14) [21] at J-PARC MLF. Only the data under transverse US injection at 64.5 MHz and $\mu_0H \sim 0.1$ T along the [1 1 1] direction were taken at AMATERAS. In Fig. 1, the horizontal scattering plane was the same as that of DNA. With and without the US injection, the magnetic Bragg peak measurement at $02\bar{2}$ was carried out from 5 K
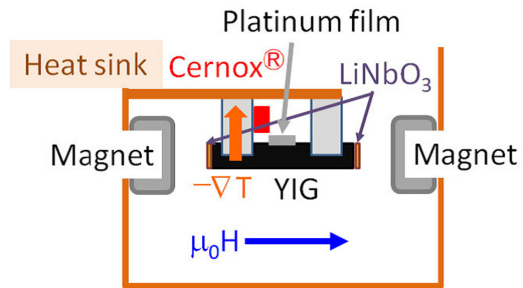
to 300 K at $E_i= 3.1$ meV for around 20 min. For most of our measurements at DNA, Si(111) reflection was used as the analyzer and a pulse-shaping chopper with a 3-cm slit at a rotating speed of 225 Hz was used resulting in an energy resolution of 3.4 μeV at $E = 0$ meV. The final energy E_f of DNA with Si(111) analyzer was 2.08 meV. The vertical Q resolution was about 0.02 Å^{-1}. A pulse-shaping chopper with a 1-cm slit and a rotating speed of 300 Hz was utilized to get a high energy resolution of 1.6 μeV at $E = 0$ meV for US frequency dependence measurement of the magnetic Bragg peak at DNA. The US amplitude dependence was measured by Si(111) analyzer with a 3-cm slit at a rotating speed of 300 Hz. The intensity around $02\bar{2}$ was integrated with the range of ±0.05 r.l.u. in Q_a, ±0.04 r.l.u. in Q_b, and ±0.075 r.l.u. in Q_c. $02\bar{2}$ is the strongest magnetic Bragg peak, which includes a nuclear Bragg component with 2.7% of the total intensity. As a reference, the nuclear Bragg peak at 642 was measured by Si(333) analyzer with a 3-cm slit at a rotating speed of 225 Hz. The intensity also includes a small magnetic Bragg component with 1.1% of the total intensity. The neutron scattering measurements were carried out under a proton beam power of 300–600 kW at J-PARC.

UTSUSEMI software is used for the analysis of the data sets [22]. QENSFIT software is used for the energy-width analysis of the magnetic Bragg peak $02\bar{2}$ [23]. The errors are estimated as standard deviations.

Sample cell configuration is shown in Fig. 2. A magnetic field of about 0.1 T was applied along the crystal rod direction to remove magnetic domain walls by a pair of permanent magnets. Based on an ellipsoidal approximation, the magnetic field configuration along the cylindrical rod direction reduces the demagnetizing field coefficient below 4% for our crystals. The magnetic field directions were parallel to the US propagation vector **k** and the crystal rod directions for neutron scattering measurements. At the magnetic Bragg point $02\bar{2}$, the magnetic field direction is normal to the scattering vector **Q**. To avoid probable neutron detector errors at DNA, the outside magnetic field at 30 cm away from the sample position was suppressed down to roughly 0.1 mT by creating a permalloy magnetic circuit through the crystal.

US wave was generated by LiNbO$_3$ thin crystal with gold leads for both sides of a YIG crystal. Two types of glues were used depending on the measuring temperatures. Below 200 K, room-temperature-vulcanizing (RTV) silicone rubber (Shinetsu Co., Ltd.) was used to glue the YIG crystal and the LiNbO$_3$ transducer. For high-temperature measurements above 150 K, however, the Aron Alpha jerry-type (Toagosei Chemical Industry Co., Ltd.) was employed. The US echo was detected by a LiNbO$_3$ transducer at the other side of the YIG crystal. During the neutron scattering measurements, the US wave was continuously injected in YIG at a peak-to-peak voltage V_{pp} of 10 V or 20 V, forming a standing wave by adjusting the frequency. We studied the following four configurations. Transverse and longitudinal modes were injected into two cylindrical YIG crystals grown along [1 1 1] and [0 0 1]. The US propagation vector **k** was parallel to the crystal rod direction, whereas the vibration vector **u** was changed depending on the US mode. Here, the four US conditions are abbreviated as follows. μ_0**H** $\parallel$ **k** $\parallel$ **u** $\parallel$ [0 0 1] is [0 0 1]L. μ_0**H** $\parallel$ **k** $\parallel$ [0 0 1] and **u** $\parallel$ [1 0 0] is [0 0 1]T. μ_0**H** $\parallel$ **k** $\parallel$ **u** $\parallel$ [1 1 1] is [1 1 1]L. μ_0**H** $\parallel$ **k** $\parallel$ [1 1 1] and **u** $\parallel$ [1 -1 0] is [1 1 1]T. They correspond to the elastic constants, C_{11}, C_{44}, $(C_{11} + 2C_{12} + 4C_{44})/3$, and $(C_{11} - C_{12} + C_{44})/3$, respectively. Note that the LiNbO$_3$ transducer size was unified for most of the measurements except for the [0 0 1]L case in Fig. 5(a), where the area size was about a quarter of the other, leading to the small US efficiency. The straightness of US wave propagation rises when the US frequency is increased, resulting in an effective reduction of the US injected sample volume. The magnetic Bragg peak enhancement could also be influenced by the crystal quality. Because of these ambiguities, it is difficult to estimate the absolute enhancement by the US injection. Hence, we will discuss the relative change in the enhancements. SSE voltage on a platinum film with a thickness of about 20 nm on YIG was measured by 34420A micro-ohm meter (Keysight Technologies Co., Ltd.). For the neutron scattering measurements, the US transducers were attached on both ends of the cylindrical rod crystals of YIG, resulting in the US wave vector parallel to the rod direction and the magnetic field direction (Fig. 2). The SSE condition by the US has to be changed from the configuration. In this case, a transducer was mounted to the bottom side of the YIG crystal, opposite the platinum film in Fig. 2, where the US wave vector was normal to the crystal rod direction and the magnetic field, unlike the other cases. The thermal gradient was parallel to the US wave vector.

III. RESULTS AND DISCUSSION

A. Magnetic Bragg peak as a function of energy

US effects on a magnetic QENS Bragg peak at a high-resolution mode of 300 Hz are shown in Fig. 3. By applying a magnetic field along the crystal rod direction [1 1 1], the magnetic Bragg peak intensity 02$\bar{2}$ increased by 1.5 times. This change comes from the angle-dependent factor $\{1 - (\hat{\tau} \cdot \hat{\eta})^2\}_{av}$ of the elastic magnetic cross-section, where $\hat{\tau}$ is a unit vector in the direction of **Q**; $\hat{\eta}$ is a unit vector in the mean direction of the spins. It is 1 for μ_0**H** $\perp$ **Q**, while it becomes 2/3 at μ_0**H** $= 0$ because of the random magnetic domain dis-
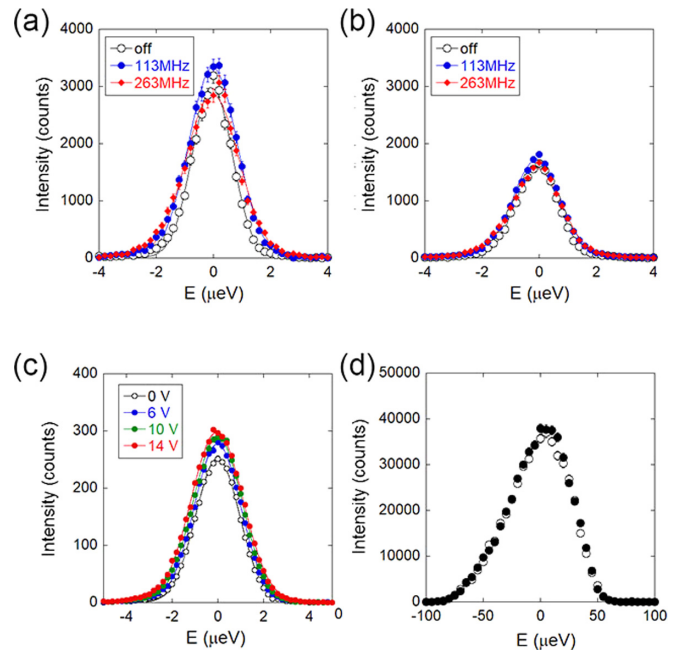

FIG. 3. Magnetic Bragg peak 02$\bar{2}$ at $T = 4-7$ K with a 1-cm slit at various frequencies of longitudinal mode US injection at (a) $\mu_0 H$ $\sim$0.1 T along the [1 1 1] direction and (b) 0 T. (c) US amplitude dependence of the magnetic Bragg peak at $f = 113.1$ MHz of [1 1 1]L with a 3-cm slit. (d) Nuclear Bragg peak at 642 measured under 113.1 MHz US injection of [1 1 1]L at 5.4 K. Solid lines are a guide to the eyes.

tribution [20,24]. The large intensity change suggests that the magnetic domain walls of YIG are fully removed. Under the magnetic field, the full width of half maximum (FWHM) became slightly narrower (93%), presumably due to the domain wall effect. For example, the FWHM under the US injection of 263.3 MHz at $\mu_0 H = 0$ became 6% wider than that without US injection [Fig. 3(b)]. The integrated intensity increased by 14 ± 1%. On the other hand, the nuclear Bragg peak intensity of 642 increased only by 3 ± 3% [Fig. 3(d)]. The FWHM changed from 53 ± 1 to 52 ± 1 μeV. Both changes were small within the errors. The results suggest that the phonon created by the US does not affect the nuclear Bragg peak intensity. The small change contrasts with the increases in magnetic Bragg peak intensity shown in Figs. 3(a)–3(c), suggesting that the observed enhancement in the magnetic Bragg peak by the US injection is originated from the magnetic effect.

Deconvoluted energy width ΔW was estimated by a numerical deconvolution software QENSFIT [23]. The original magnetic Bragg peak without the US injection was assumed as a resolution-limited peak for the deconvolution. After various trials, we found that the energy width ΔW in the deconvoluted dynamical structure factor $S_d(E)$ is well expressed by the sample temperature increase ΔT under the US injection as follows:

$$S_d(E) = S_0 \exp\left(-\frac{4\ln(2)E^2}{\Delta W^2}\right),\tag{1}$$
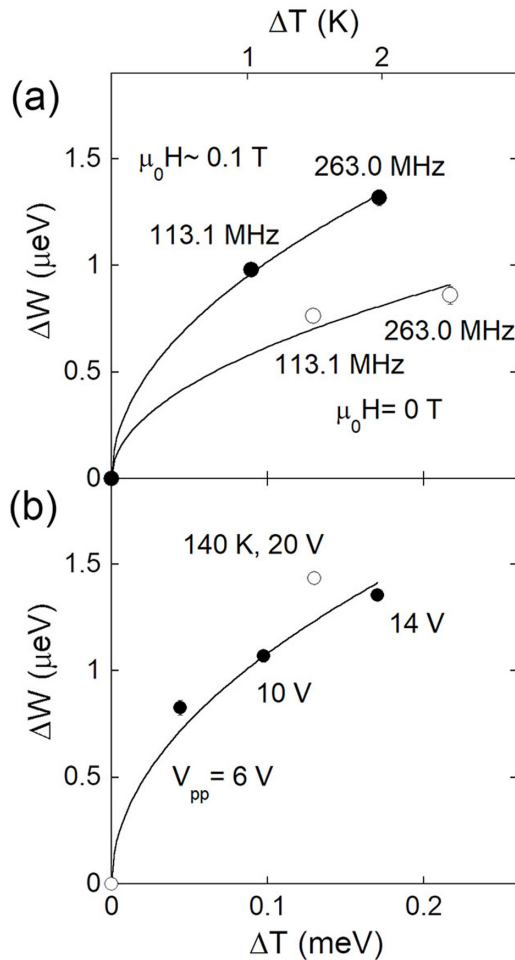
$$\Delta W = \sqrt{Ak_B \Delta T},\tag{2}$$

FIG. 4. (a) Deconvoluted energy width ΔW at various US frequency (μeV) as a function of ΔT at $\mu_0 H \sim 0.1$ T along the [1 1 1] direction (closed circles) and 0 T (open circles). (b) Deconvoluted energy width ΔW (closed circles) at various US amplitude V_{pp} (V) as a function of ΔT. ΔW value at about 140 K (open circle) is added as a reference. Solid lines are fitting by Eq. (2).

where A is a constant and ΔT is the sample temperature increase by the US injection. The ΔT in Fig. 2 is measured by the Cernox sensor as the difference between the US on and off. The sensor position is very close to the 25-ohm resistive heater and the YIG sample within 2 cm in dilute He gas. The fitted results by Eq. (2) are shown in Fig. 4.

The US injection could cause some radio-wave emission from the electrical wires, particularly at high frequencies, resulting in power loss. Then, for the injected power into the sample, the US sample temperature increases ΔT can be a good measure. However, the injected power δQ is proportional to $C_p \delta T$, where C_p is the specific heat capacity of YIG at a constant pressure. C_p of YIG increases twice in the temperature range 4 to 7 K [15]. As a result, the ΔW increases not with the injected power δQ, but with the ΔT. Note that the ΔW does not increase simply with increasing the sample temperature. The magnetic Bragg peak is broadened only by the US injection. At present, there is no relevant theoretical equation for QENS peak broadening under US injection. According to a liquid model of QENS with a Gaussian ap-

proximation in short times, however, the ΔW is proportional to the square root of the effective temperature T_0 as expressed by $\Delta W = 4\sqrt{\ln(2)E_r k_B T_0}$ [25], where the recoil energy $E_r = \hbar^2 Q^2/(2m_0) = 78$ μeV for Fe standard atomic weight of $m_0 = 55.847$ at $Q(02\bar{2}) = 1.44$ Å^{-1}. In the present US injection, the effective temperature T_0 is replaced by the increased sample temperature ΔT, which is induced solely by the US injection. Furthermore, the peak center did not shift by the recoil energy E_r expected for scattering from a single free nucleus, suggesting that the Fe atoms are strongly bonded to the lattice as a solid in YIG. Meanwhile, the deconvoluted energy width ΔW by the US injection becomes proportional to the square root of the US sample temperature increase $\sqrt{\Delta T}$ for both the frequency and amplitude dependencies. Note that the ΔW at about 140 K was 1.43 ± 0.02 μeV at $k_B \Delta T = 0.13$ meV by the US injection of [1 1 1]T with 21.0 MHz and $V_{pp} = 20$ V. The value was fairly close to the fitting line in Fig. 4(b), suggesting that the relationship may be applied at various temperatures. The current significant correlation between energy-width and temperature increase ΔT by the US suggests that the US-induced lattice vibration can be regarded as a particle vibration in a liquid by QENS.

The energy width ΔW of the magnetic Bragg peak $02\bar{2}$ is related to the spin arrangement, whereas the US injection becomes a phonon injection. The energy width can change by the phonon injection only through a spin-lattice coupling. By fitting the data based on Eq. (2), the constant values A were estimated as 10.3 ± 0.2 neV at $\mu_0 H = 0.1$ T and 3.8 ± 0.4 neV at $\mu_0 H = 0$ T for Fig. 4(a), and 11.7 ± 0.9 neV for Fig. 4(b), whereas $A = 16\ln(2)E_r = 861$ μeV in the liquid model. The parameter A in the liquid model is proportional to the recoil energy at the fixed measuring Q point. For the value A, the relationship leads to the effective mass M of the magnetic Fe atom. Then 10.3, 3.8, and 11.7 neV correspond to $M = 83.3$, 226.4, and $73.7 \times 10^3 m_0$, respectively. The effective masses were extremely heavy. The effective mass becomes light under the magnetic field because of the absence of magnetic domain walls. ΔT increases with increasing US frequency or voltage, resulting in a broader energy width of the magnetic Bragg peak.

B. Magnetic Bragg peak intensity as a function of temperature

Magnetic Bragg peak $02\bar{2}$ was largely enhanced at low temperatures by the US injection. The enhancement was studied by using four US modes, [0 0 1]L, [0 0 1]T, [1 1 1]L, and [1 1 1]T. The magnetic Bragg peak enhancement showed irreversible behavior after the US injection for both the temperature and amplitude scans. The large irreversibility in the temperature scan was observed up to 20%. On the other hand, the irreversibility in the amplitude scan was below 5%. They suggest large strains remaining in the lattice. When a stress exceeds an elastic limit, the strain persists, widening the mosaic spread. It increases the Bragg peak intensity, corresponding to the dynamical theory of diffraction [2].

The temperature dependence of the enhancement ratio is shown in Fig. 5. The data show a broad scatter when US injection was switched on and off at each temperature as shown in Fig. 5(b). When the data were taken keeping only with US injection (or without US injection) during the temperature
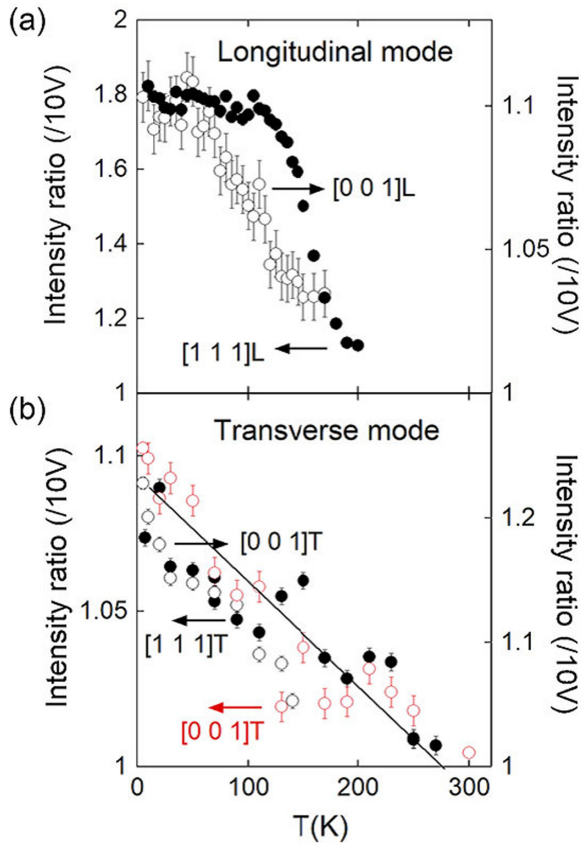
FIG. 5. Temperature dependence of enhancement ratio on the magnetic Bragg peak intensity of $02\bar{2}$ by US injection of longitudinal (a) and transverse (b) modes at $V_{pp} = 10$ V. Closed symbols are US **k** ∥ [**1 1 1**], whereas open symbols are US **k** ∥ [**0 0 1**]. US frequencies are 36.3 MHz for [1 1 1]L (closed black circles), 34.3 MHz for [0 0 1]L (open black circles) (a), 64.5 MHz for [1 1 1]T (closed black circles), 113.3 MHz for [0 0 1]T (open black circles), and 67.6 MHz for [0 0 1]T (open red circles) (b). The solid line is a guide to the eye.

scan, the broad scatter was reduced, which may be attributed to the strain effect [Fig. 5(a)]. Although the enhancement ratio showed strong temperature dependence, the magnetic Bragg peak intensity of $02\bar{2}$ decreased only by 5% from 10 K to 300 K at $\mu_0 H \sim 0.1$ T along the [1 1 1] direction. This is because YIG has a Curie temperature of 560 K much higher than room temperature.

The peak enhancement by longitudinal mode is generally more significant than that by transverse mode after taking into account the small transducer size for [0 0 1]L. The result is consistent with the original discussion of US acoustic spin pumping [6]. The enhancement ratio of the transverse mode decreases monotonously with temperature despite the scattered data, but the longitudinal mode displays a sharp drop over 100 K. The enhancement of the transverse mode becomes negligibly small at room temperature. This contrasts with a result obtained by x-ray diffraction on Si and Ge where a large enhancement ratio is observed even at room temperature [1,4].

The integrated intensity of the magnetic Bragg peak $02\bar{2}$ is the product of the energy-width multiplied by the peak intensity. The energy width of the magnetic Bragg peak was shown to be strongly connected to the US sample temperature

increase ΔT in the previous section. The dynamical scattering effect, as demonstrated by x-ray diffraction on Si and Ge crystals, is responsible for the peak intensity enhancement [1,4]. Let us assume that the magnetic Bragg peak intensity is enhanced solely by the thermal effect ΔT. Although V_{pp} was fixed during the temperature scan, the thermal effect of ΔT may become small at high temperatures. This could be one of the reasons for the reduction of the magnetic Bragg peak enhancement with increasing temperature as shown in Fig. 5. However, the sharp decrease from 100 K to 200 K in the magnetic Bragg peak enhancement in Fig. 5(a) cannot be compensated by the thermal effect, suggesting the significant decrease in the spin-lattice coupling above 100 K.

C. Spin Seebeck effect and acoustic spin pumping

The spin Seebeck voltage is enhanced by the magnon polaron (magnetelastic wave) effect, suggesting the importance of the spin-lattice coupling [12,26]. The thermal SSE is based on the spin current produced by the thermal flow in a sample. The thermal flow in YIG has two components, which are magnon and phonon. Although the magnon thermal conductivity may dominate at low temperatures below 20 K, the phonon carries the majority of the thermal flow above 20 K [27,28]. If we consider the parallel circuit of magnon and phonon thermal flows, the magnon contribution becomes negligible in the thermal flow above 20 K. However, the spin Seebeck voltage does not decrease above 20 K. Under the condition, the spin-lattice coupling must play a significant role in the spin Seebeck voltage above 20 K. If the spin-lattice coupling effect is strong in the SSE, the phonon flow may often be converted to the magnon flow at the interface of YIG and Pt.

The thermal SSE is degraded above 100 K. It has previously been attributed to spectral nonuniformity of magnon thermalization lengths in the thermospin conversion [12], as well as an increase in magnon-magnon scattering at high temperatures [14]. Because the mean free path of a phonon in YIG reduces by several orders of magnitude from 10 K to 160 K, the mean free path of a magnon should also decrease [28]. However, the ultralow-energy magnon spectra below 45 μeV of YIG changed a little from 50 K to 300 K, suggesting small magnon-magnon scattering even at 300 K in this low-energy range [15]. Meanwhile, the temperature dependence of spin-lattice coupling has not been considered in the SSE. The current sharp drop in magnetic Bragg peak enhancement over 100 K in Fig. 5(a) indicates that the spin-lattice coupling in YIG has significantly deteriorated. In other words, the SSE induced by the US injection could be largely enhanced with decreasing temperature. However, it is difficult to understand the large spin-lattice coupling only in the high-spin state of $Fe^{3+}(3d^5)$ ion with no angular momentum. One of the possible origins can be attributed to $Fe^{2+}(3d^6)$ impurity effect because of the unquenched angular momentum [16]. A small number of excess electrons form magnetically anisotropic Fe^{2+} ions freezing below 150 K. It can lead to the enhancement of spin-orbit coupling. We observed a magnetization anomaly below 150 K, suggesting the spin canting in YIG [15]. As a result, the abrupt increase in the magnetic Bragg peak enhancement observed below 150 K can be interpreted
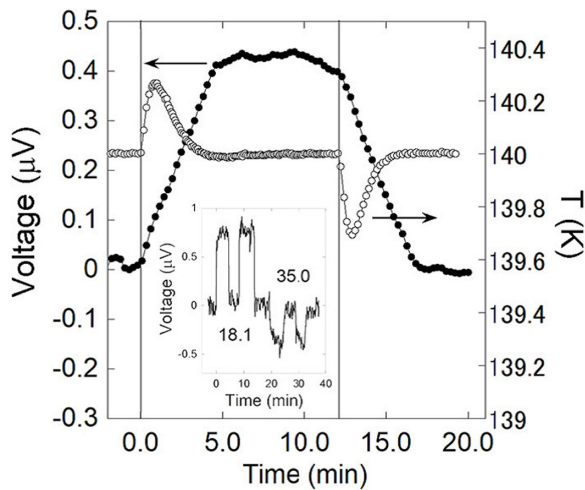
FIG. 6. Voltage of thermal gradient SSE (closed circles) at $\mu_0 H \sim 0.1$ T along the [1 1 1] direction as a function of time at $T = 140$ K. The longitudinal US injection of 36.3 MHz starts at $t = 0$ then stops at $t = 12$ min. The temperature (open circles) at the YIG crystal is shown on the right-hand axis. Inset shows voltage sign change of ultrasound SSE with increasing frequency at $\mu_0 H \sim -0.1$ T. Before 17 min, 18.1 MHz US was applied two times, while 35.0 MHz US was applied two times after 17 min.

as the emergence of significant spin-lattice coupling below 150 K.

The SSE was measured at $T = 140$ K on a Pt film with a thickness of about 20 nm on the YIG crystal in the same setup as the QENS measurement (Fig. 2). The longitudinal US was injected along [1 1 1] with a frequency of 36.3 MHz at $\mu_0 H \sim 0.1$ T. During the US injection, the SSE voltage appeared as shown in Fig. 6. The SSE voltage was measured along [0 1 −1], while the magnetic field was applied along [1 1 1]. The crystal temperature was monitored by a Cernox temperature sensor attached to the aluminum pillar in Fig. 2.

The temperature at one side of the YIG crystal is shown by open circles in Fig. 6. During the thermal equilibration, the SSE monotonically increased, suggesting that the origin of SSE voltage is the thermal gradient ∇T (Fig. 2). The US heat was absorbed into the aluminum pillar. The temperature gradient direction [2 −1 −1] was normal to both the [1 1 1] and the voltage direction [0 1 −1] on the platinum film. This configuration is the same as the SSE measurements by a thermal gradient [12]. The magnetic Bragg peak enhancement [closed black circles in Fig. 5(a)] under the same condition of Fig. 6 confirms the strong US injection effect at [1 1 1]L.

Acoustic spin pumping (ASP) configuration of $\mu_0 \mathbf{H} \parallel$ [1 1 1] and $\mathbf{k} \parallel \mathbf{u} \parallel [1 -1 \, 0]$ was also tested. In this case, we observed SSE sign change with decreasing frequency from

35.0 MHz (positive SSE voltage) to 18.1 MHz (negative SSE voltage). The sign change is consistent with the US ASP observed at a low frequency such as 3.5 MHz [7]. Furthermore, the SSE voltage at 18.1 MHz begins to change significantly faster than that at 35.0 MHz, in contrast to the slow thermal gradient SSE voltage increase shown in Fig. 6. The quick change is consistent with the expected US ASP effect within 1 μsec [8]. The present configuration is different only in the crystal axis from the original unique configuration $\mathbf{k} \parallel \mathbf{u} \parallel$ [**1 1 1**] $\perp \mu_0 \mathbf{H}$ [7]. The original [1 1 1]L condition coincides with the large enhancement case in Fig. 5. So far, the QENS signal difference between SSE and ASP has not been observed.

Here, low US frequencies were used for the SSE measurement to observe the US effect. However, the high US frequency can largely change the magnetic Bragg peak as shown in Fig. 4(a). Hence, the high US frequencies were used in the previous neutron scattering measurements.

IV. CONCLUSIONS

Ultrasound effects were studied by quasielastic neutron scattering on yttrium iron garnet, where the ultrasound is injected as a standing wave of longitudinal or transverse mode. The ultrasonic injection significantly increased the magnetic Bragg peak intensity at low temperatures. The enhancement decreased with increasing temperature, notably above 100 K, suggesting the strong temperature dependence of the spin-lattice coupling for the longitudinal mode in the temperature range. The quasielastic neutron scattering under ultrasound injection can be a powerful tool to study the spin-lattice coupling in a magnet. This method has relatively high efficiency as neutron scattering because the measurement takes only a short time such as 10–20 min at each temperature. Meanwhile, the energy-width measurement with a high-resolution mode takes about 5 hours at each condition.

[1] K.-D. Liss, A. Magerl, A. Remhof, and R. Hock, Ultrasound-induced gradient crystals observed by high-energy x-rays, Acta Crystallogr. Sect. A **53**, 181 (1997).

[2] W. H. Zachariasen, *Theory of X-ray Diffraction in Crystals* (John Wiley & Sons, London 1945).

[3] E. Iolin, B. Farago, F. Mezei, E. Raitman, and L. Rusevich, Inelastic neutron scattering on the high-frequency ultrasound

in single crystals, Phys. B: Condens. Matter **241–243**, 1213 (1997).

[4] A. Remhof, K.-D. Liss, and A. Magerl, Neutron diffraction from sound-excited crystals, Nucl. Instrum. Methods Phys. Res., Sect. A **391**, 485 (1997).

[5] K. Uchida, H. Adachi, T. An, T. Ota, B. Hillebrands, S. Maekawa, and E. Saitoh, Long-range spin Seebeck effect and acoustic spin pumping, Nat. Mater. **10**, 737 (2011).

[6] K. Uchida, H. Adachi, T. Ota, H. Nakayama, S. Maekawa, and E. Saitoh, Observation of longitudinal spin-Seebeck effect in magnetic insulators, Appl. Phys. Lett. **97**, 172505 (2010).

[7] K. Uchida, H. Adachi, T. An, H. Nakayama, M. Toda, B. Hillebrands, S. Maekawa, and E. Saitoh, Acoustic spin pumping: Direct generation of spin currents from sound waves in Pt/Y$_3$Fe$_5$O$_{12}$ hybrid structures, J. Appl. Phys. **111**, 053903 (2012).

[8] M. Weiler, H. Huebl, F. S. Goerg, F. D. Czeschka, R. Gross, and S. T. B. Goennenwein, Spin Pumping with Coherent Elastic Waves, Phys. Rev. Lett. **108**, 176601 (2012).

[9] E. Saitoh, M. Ueda, H. Miyajima, and G. Tatara, Conversion of spin current into charge current at room temperature: Inverse spin-Hall effect, Appl. Phys. Lett. **88**, 182509 (2006).

[10] A. Azevedo, L. H. Vilela Leao, R. L. Rodriguez-Suarez, A. B. Oliveira, and S. M. Rezende, dc effect in ferromagnetic resonance: Evidence of the spin-pumping effect? J. Appl. Phys. **97**, 10C715 (2005).

[11] K. Uchida, S. Takahashi, K. Harii, J. Ieda, W. Koshibae, K. Ando, S. Maekawa, and E. Saitoh, Observation of the spin Seebeck effect, Nature (London) **455**, 778 (2008).

[12] T. Kikkawa, K. Shen, Benedetta F., R. A. Duine, K.-I. Uchida, Z. Qiu, G. E. W. Bauer, and E. Saitoh, Magnon Polarons in the Spin Seebeck Effect, Phys. Rev. Lett. **117**, 207203 (2016).

[13] T. Kikkawa, K.-I. Uchida, S. Daimon, Z. Qiu, Y. Shiomi, and E. Saitoh, Critical suppression of spin Seebeck effect by magnetic fields, Phys. Rev. B **92**, 064413 (2015).

[14] J. Barker and G. E. W. Bauer, Thermal Spin Dynamics of Yttrium Iron Garnet, Phys. Rev. Lett. **117**, 217201 (2016).

[15] S. Shamoto, Y. Yasui, M. Matsuura, M. Akatsu, Y. Kobayashi, Y. Nemoto, and J. Ieda, Ultralow-energy magnon anomaly in yttrium iron garnet, Phys. Rev. Res. **2**, 033235 (2020).

[16] Y. Yamasaki, Y. Kohara, and Y. Tokura, Quantum magneto-electric effect in iron garnet, Phys. Rev. B **80**, 140412(R) (2009).

[17] K. Shibata, N. Takahashi, Y. Kawakita, M. Matsuura, T. Yamada, T. Tominaga, W. Kambara, M. Kobayashi, Y. Inamura, T. Nakatani *et al.*, The performance of TOF near backscattering spectrometer DNA in MLF, J-PARC, JPS Conf. Proc. **8**, 036022 (2015).

[18] S. Kimura and I. Shindo, Single crystal growth of YIG by the floating zone method, J. Cryst. Growth **41**, 192 (1977).

[19] D. Rodic, M. Mitric, R. Tellgren, H. Rundlof, and A. Kremenovic, True magnetic structure of the ferrimagnetic garnet Y$_3$Fe$_5$O$_{12}$ and magnetic moments of iron ions, J. Magn. Magn. Mater. **191**, 137 (1999).

[20] S. Shamoto, T. U. Ito, H. Onishi, H. Yamauchi, Y. Inamura, M. Matsuura, M. Akatsu, K. Kodama, A. Nakao, T. Moyoshi, K. Munakata, M. Nakamura, S. Ohira-Kawamura, Y. Nemoto, and K. Shibata, Neutron scattering study of yttrium iron garnet, Phys. Rev. B **97**, 054429 (2018).

[21] K. Nakajima, S. Ohira-Kawamura, T. Kikuchi, M. Nakamura, R. Kajimoto, Y. Inamura, N. Takahashi, K. Aizawa, K. Suzuya, and K. Shibata, AMATERAS: A cold-neutron disk chopper spectrometer, J. Phys. Soc. Jpn. **80**, SB028 (2011).

[22] Y. Inamura, T. Nakatani, J. Suzuki, and T. Otomo, Development status of software "Utsusemi" for chopper spectrometers at MLF, J-PARC, J. Phys. Soc. Jpn. **82**, SA031 (2013).

[23] T. Yamada, *QENSfit*, https://youtu.be/RTZWv6BH7mQ, in Japanese.

[24] G. L. Squires, *Inroduction to the Theory of Thermal Neutron Scattering* (Cambridge University Press, Cambridge, 1978).

[25] B. R. A. Nijboer and A. Rahman, Time expansion of correlation functions and the theory of slow neutron scattering, Physica **32**, 415 (1966).

[26] N. Ogawa, W. Koshibae, A. J. Beekman, N. Nagaosa, M. Kubota, M. Kawasaki, and Y. Tokura, Photodrive of magnetic bubbles via magnetoelastic waves, Proc. Natl. Acad. Sci. USA **112**, 8977 (2015).

[27] R. L. Douglass, Heat Transport by Spin Waves in Yttrium Iron Garnet, Phys. Rev. **129**, 1132 (1963).

[28] S. R. Boona and J. P. Heremans, Magnon thermal mean free path in yttrium iron garnet, Phys. Rev. B **90**, 064421(R) (2014).